Inorganic Chemistry

Article

pubs.acs.org/IC

Octacoordinated Dioxo-Molybdenum Complex via Formal Oxidative Addition of Molecular Oxygen. Studies of Chemical Reactions Between $M(CO)_6$ (M = Cr, Mo) and 2,4-Di-*tert*-butyl-6-(pyridin-2-ylazo)-phenol

Ipsita Chatterjee,[†] Nabanita Saha Chowdhury,[†] Pradip Ghosh, and Sreebrata Goswami*

Department of Inorganic Chemistry, Indian Association for the Cultivation of Science, Jadavpur, Kolkata-700032, India

Supporting Information

ABSTRACT: Reactions of $M(CO)_6$ (M = Mo, Cr) and 2 mol of 2,4-di-*tert*-butyl-6-(pyridin-2-ylazo)-phenol ligand (HL) in air yielded $[Mo^{VI}O_2(L^{1-})_2]$, **1**, and $[Cr^{III}(L^{1-})(L^{\bullet 2-})]$, **2**, respectively, in high yields. Formation of the Cr-complex is a substitution reaction, which is associated with electron transfer, while that of Mo is an example of molecular oxygen activation. Isolated monoradical chromium complex **2** is susceptible to oxidation. Accordingly the reaction of **2** with the oxidant, I_2 produces a cationic nonradical complex of chemical composition $[Cr^{III}(L^{1-})_2]I_3$, $[\mathbf{2}]I_3$ in almost quantitative yield. All the isolated complexes are primarily characterized by various spectroscopic techniques and magnetic measurements. While the molybdenum complex is diamagnetic, the two chromium complexes behave as simple paramagnets: μ_{eff} (295 K), 2.81 μ_B and 3.79 μ_B for **2** and $[\mathbf{2}]I_3$, respectively. Single-crystal three-dimensional X-ray structures of **1**, **2**, $[\mathbf{2}]I_3$ are reported. The geometry of the Mo-complex is square antiprism (octacoordination), and that of the Cr-complexes is distorted octahedral. Redox properties of the complexes are studied by cyclic voltammetry and constant potential coulometry. The data are analyzed based on density functional theoretical calculations of molecular orbitals of redox isomers of the Cr complexes. The results indicated that the redox events in the complexes occur at the ligand center. The oxidation state of Cr in **2** is further assessed by XPS measurements and compared with the reported systems.

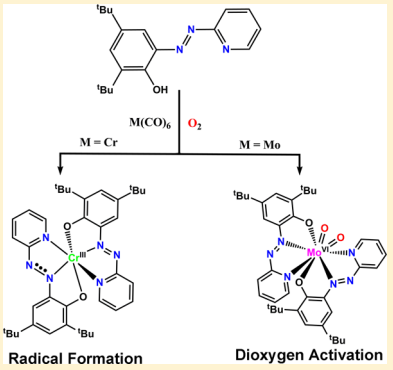

INTRODUCTION

In recent years, there has been considerable interest in the transition metal complexes of redox noninnocent azoaromatic ligands particularly because of their versatile chemical reactivity. For example, regioselective hydroxylation,[1] thiolation,[2] and amination[3] reactions by *ortho*-$C_{aromatic}$-H activation were reported during the last three decades, and more recently their participation in chemical catalysis[4] involving ligand redox has been realized. Though it has been known since long ago that the azo-centered π^* molecular orbital of the azo aromatic ligands is low-lying and can be directly populated by one or two electrons, chemically or electrochemically, the azo-anion radical oxidation state in stable complexes were reported much later.[5] Furthermore, chemical transformations of this class of ligands by reductive cleavage[6] ($4e^-$ transfer) of azo function vis-á-vis metathesis reactions[7] are also demonstrated in current literature.

Principal objective of this report is to disclose formal oxidative addition of dioxygen to a molybdenum center via a hypersensitive molybdenum complex intermediate of an azoaromatic ligand, 2,4-di-*tert*-butyl-6-(pyridin-2-ylazo)-phenol (HL) (Scheme 1). This class of reaction is important[8] with respect to catalyzed oxygen atom transfer (OAT) to another substrate with direct participation[9,10] of aerial oxygen. The conversion $O_2 \rightarrow 2O^{2-}$ is a net $4e^-$ reduction process, which usually occurs in bimetallic systems[11,12] resulting in $2e^-$ oxidation of each metal fragment.

Scheme 1

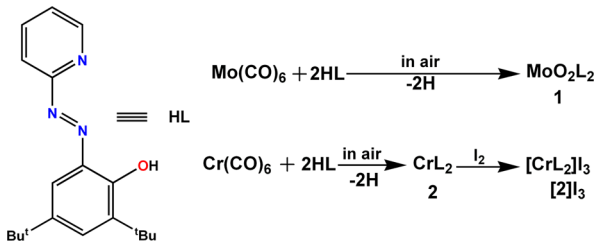

To gain some knowledge on the identity of the aforesaid Mo intermediate in the above reaction, we examined the chemical behavior of closely related Cr complex. We report, herein, two parallel reactions of $M(CO)_6$ (M = Mo and Cr) with the above ligand in air. The reaction of Mo^0 yielded an octacoordinated blue complex MoO_2L_2, while that of Cr^0 yielded a hexacoordinated monoradical complex of composition CrL_2. Notably the unique eight CN of a monometallic Mo complex[13] appears to be among the least abundant, accounting for <1% of

Received: January 29, 2015
Published: May 15, 2015

DOI: 10.1021/acs.inorgchem.5b00218
Inorg. Chem. 2015, 54, 5257−5265

all transition-metal complexes reported in the CSD (version 5.30). Characterization of the isolated Cr complexes and electrogenerated redox partners are scrutinized thoroughly by spectroscopic techniques and density functional theory (DFT).

RESULT AND DISCUSSION

The organic ligand (HL), used herein, belongs to a well-known family of a dye pyridylazonapthol (PAN), whose use in analytical chemistry has been known since long ago.[14] The coordination chemistry of this and closely related ligands are also available in the literature.[15] These offer three very different kinds of coordination, specifically, a pyridyl-N, a reducible azo function, and an oxidizable hydroxo-O (after deprotonation). Pyridyl-N and hydroxo-O are strongly donating, while azo-N is π-accepting. A line drawing of the ligand HL and the isolated complexes are collected in Scheme 1.

We recently[4a,16] have shown that the reactions of electron-rich metal precursors and azo-aromatic ligands in general produce azo-anion radical complexes directly. In selective instances multiple electron reductions occur as happened in the reaction between $Re_2(CO)_{10}$ and HL, which led to reductive cleavage of the azo function.[7] In this work we used M^0 carbonyls (M = Cr, Mo) as starting materials for the chemical synthesis of metal complexes with the anticipation that substitution of CO together with redox reaction between the electron-rich metal (M^0) and the acceptor ligand(s) would set in for the formation of the final product.

Syntheses of Metal Complexes. The present work began with a chemical reaction between $Mo(CO)_6$ and 2 mol of HL in octane and in air, which resulted in an intensely blue colored octacoordinated cis-dioxo complex. An identical reaction in deaerated conditions produced a hypersensitive brown complex (**I**), which we could not isolate or characterize fully. However, the exposure of this intermediate to air produced the above dioxo complex, MoO_2L_2, rapidly (2−3 min) indicating formal oxidative addition of O_2 at the intermediate (**I**). A spectral trace of formation of the complex **1** from the brown intermediate (**I**) is shown in Figure 1.

To establish unequivocally that dioxygen is the source of the terminal oxygen atoms in **1**, isotope labeling experiments using ^{18}O was performed, and the electrospray ionization−mass spectrometry (ESI-MS) as well as IR spectra were analyzed.

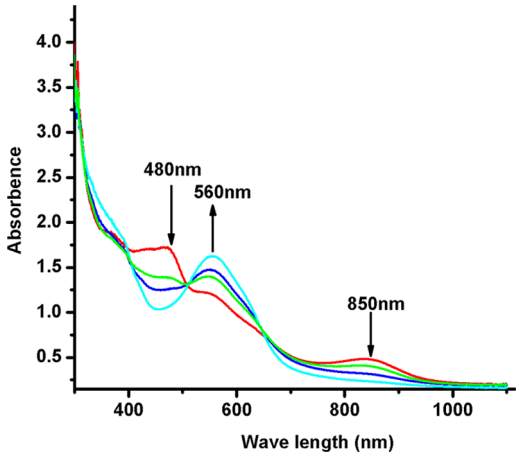

Figure 1. UV−vis spectral changes during the conversion: brown solutuion of the intermediate in toluene (red) upon exposure to air produces the final product (cyan).

The ESI-MS spectrum of compound **1** displayed a weak molecular ion peak of $[HMoO_2L_2]^+$ at m/z 751 amu associated with another major peak of $[MoO_2L]^+$ at m/z 440 amu. The $^{18}O_2$-labeled sample displayed a similar spectral pattern but with a positive shift of four amu units at m/z 755 and 444 amu, respectively. The mass spectrum of $^{16}O_2$-labeled compound matched well with the simulated one; however, there is a mismatch between the experimental and simulated spectra of $^{18}O_2$-labeled sample, which is due to the contamination of $^{16}O_2$ with the $^{18}O_2$ in our reaction conditions. A similar observation was also noted in the $^{18}O_2$-labeled spectrum of $[MoO_2L]^+$ (Supporting Information, Figure S1). The molecular ion peaks are displayed in Figure 2 and Supporting Information, Figure S1.

Furthermore, the Mo complex shows two sharp signals in the IR spectrum at 870 and 890 cm^{-1} due[17a] to $\upsilon_{Mo=O}$ for a cis $Mo(O^{16})_2$ moiety, and that in the corresponding ^{18}O-labeled species appears as an unresolved broad band appearing in the range of 775−835 cm^{-1} (Supporting Information, Figure S2). This observation of bathochromic shift of IR frequency together with ESI-MS spectral shift, both are indicative[17b] of O_2 addition for the formation of the compound **1** from the above reaction. Broad nature of the reference band is due to mixture of isotopomers originated from the contamination of $^{16}O_2$ with $^{18}O_2$.

An identical reaction between $Cr(CO)_6$ and the ligand HL in 1:2 molar ratio in boiling *n*-octane yielded a green complex, CrL_2, **2**. One-electron oxidation of the isolated complex by iodine in a dichloromethane solvent produced the cationic complex $[CrL_2]I_3$, $[\mathbf{2}]I_3$ in nearly quantitative yield (Scheme 1). The compound **2** showed an intense peak in its ESI-MS spectrum at m/z 673 amu. All of the above complexes gave satisfactory elemental analyses (see the Experimental Section).

The molybdenum complex **1** is diamagnetic (S = 0) and displayed a highly resolved ^1H NMR spectrum in $CDCl_3$. Proton resonances of **1** along with unambiguous proton assignment of resonances is shown in Figure 3.

The two chromium complexes, on the other hand, are paramagnetic; variable-temperature magnetic susceptibility measurements were performed on polycrystalline samples of **2** and $[\mathbf{2}]I_3$ in the temperature range of 295−2 K. The dependence of their magnetic behavior on variable-temperature, effective magnetic moment μ_{eff} versus T, are shown in Supporting Information, Figure S3. The μ_{eff} values of **2** and $[\mathbf{2}]I_3$ are virtually temperature-independent from 10 to 295 K. At 295 K, the value of μ_{eff} for **2** is 2.81 μ_B, which is close to the spin-only value for an S = 1 state. The μ_{eff} value of $[\mathbf{2}]I_3$ at 295 K is 3.79 μ_B, indicating the presence of three unpaired electrons (S = 3/2).

Crystal Structure. The complexes **1**, **2**, and $[\mathbf{2}]I_3$ formed reasonable crystals for X-ray diffraction studies. Molecular view and partial atom numbering schemes of the above complexes are shown in Figures 4a,b and 5a,b, and selected bond parameters are collected in Tables 1 and 2; crystallographic details are collected in Table 3.

Single-crystal X-ray analysis of the compound **1** unambiguously established the MoN_4O_4 coordination sphere (Figure 4a). Coordination geometry around the molybdenum center may best be described as a distorted square antiprism. Two distorted squares comprising of two sets of four atoms, namely, N(3), O(1), O(4), N(4) and N(1), N(6), O(2), O(3) all coordinated at molybdenum atom form a distorted square antiprism

DOI: 10.1021/acs.inorgchem.5b00218
Inorg. Chem. 2015, 54, 5257−5265

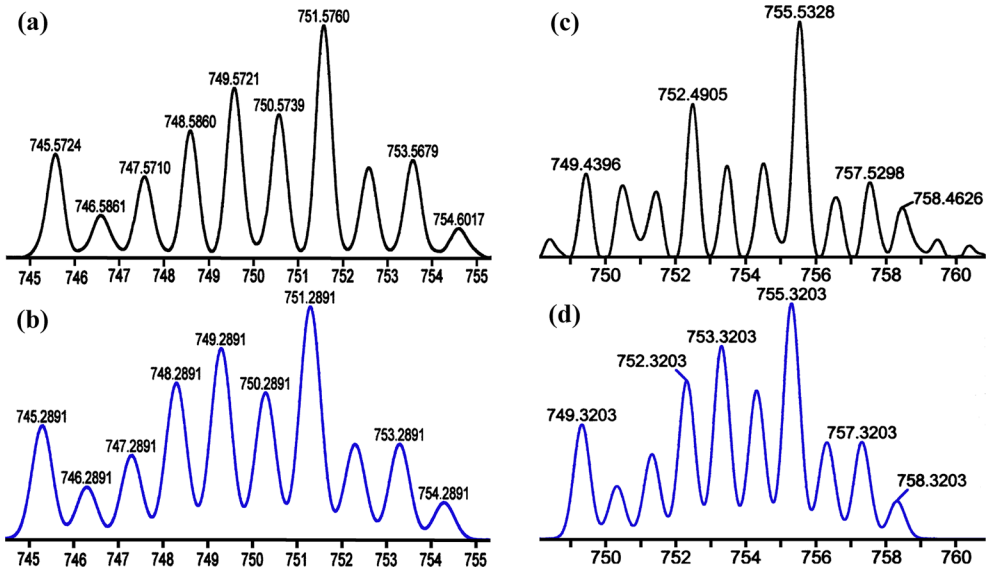

Figure 2. ESI-MS of **1** in CH_3CN: $Mo(^{16}O)_2L_2$ (a) experimental and (b) simulated; $Mo(^{18}O)_2L_2$ (c) experimental and (d) simulated.

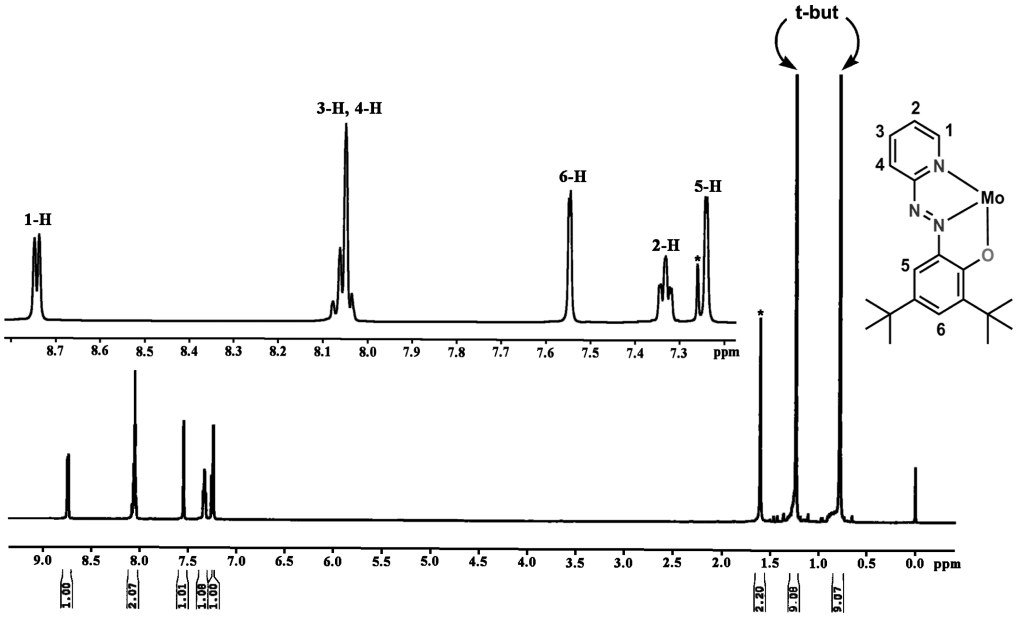

Figure 3. ^1H NMR spectrum of **1** in $CDCl_3$. (inset) Aromatic proton resonances (* from solvent).

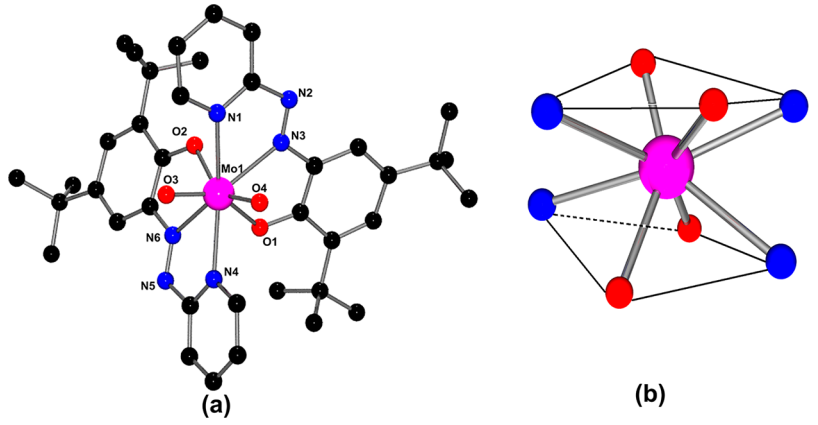

Figure 4. (a) Molecular view of the complex **1**. Hydrogen atoms are omitted for clarity. (b) Perspective view of the $[MoN_4O_4]$ core showing distorted square-antiprism geometry of the octacoordinate molybdenum complex.

DOI: 10.1021/acs.inorgchem.5b00218
Inorg. Chem. 2015, 54, 5257−5265

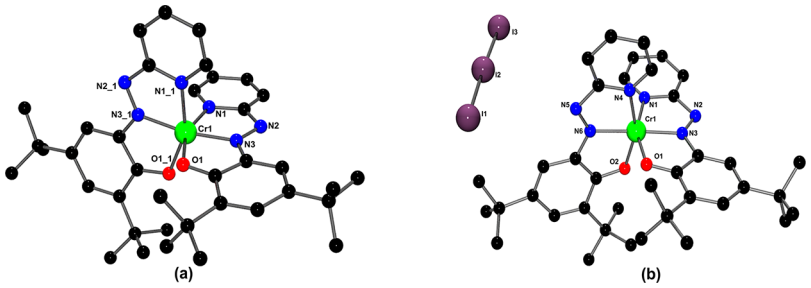

Figure 5. Molecular views of the complexes: (a) **2** and (b) $[\mathbf{2}]I_3$. Hydrogen atoms are omitted for clarity.

Table 1. Selected Bond Distances (Å) for 1 along with DFT Calculated Distances

	experimental	calculated
Mo1−O1	2.1583(12)	2.196
Mo1−O2	2.1491(13)	2.195
Mo1−O3	1.7096(12)	1.756
Mo1−O4	1.7157(12)	1.757
Mo1−N1	2.3334(15)	2.341
Mo1−N3	2.3926(14)	2.403
Mo1−N4	2.3402(15)	2.340
Mo1−N6	2.3780(15)	2.403
N2−N3	1.2747(19)	1.301
N5−N6	1.276(2)	1.301
O1−C11	1.300(2)	1.330
O2−C30	1.302(2)	1.330
N3−C6	1.373(2)	1.380
N6−C25	1.376(2)	1.380

Table 2. Selected Experimental and Computed Bond Distances of the Complexes $[Cr(L)_2]^z$ (z = 0, ±1)

	2		$[\mathbf{2}]I_3$		$[\mathbf{2}]^-$
	expt	calc	expt	cacl	calc
Cr1−N1	2.0463(17)	2.102	2.055(8)	2.094	2.125
Cr1−N4			2.043(6)	2.092	2.215
Cr1−N3	1.954(2)	2.008	1.998(7)	2.013	2.025
Cr1−N6			2.002(6)	2.013	2.025
Cr1−O1	1.9660(14)	1.943	1.933(6)	1.938	1.972
Cr1−O2			1.934(5)	1.941	1.972
N2−N3	1.323(2)	1.313	1.287(10)	1.292	1.333
N5−N6			1.297(9)	1.291	1.333
C11−O1	1.314(3)	1.319	1.315(9)	1.309	1.327
C30−O2			1.306(9)	1.308	1.327

polyhedron as shown in Figure 4b. Furthermore, the three coordinated atoms O(1), N(1), N(3) of one ligand together with one terminal oxo O(3) constitute one plane. Similarly another set of three atoms O(2), N(4), N(6) of the second ligand and another terminal oxo O(4) form another plane. These two planes are nearly perfectly orthogonal with an interplanar angle of 89.06° (Supporting Information, Figure S4). The Mo atom sits in a common position at the intersection of the aforesaid two planes.

The two chromium complexes are distorted octahedral, and the anionic ligand binds via deprotonation of OH group. The isolated molecule CrL_2 (**2**) has a crystallographic C_2 symmetry. In this structure (Figure 5a) the most notable feature is elongation of the $d_{N=N}$ bonds of the azo chromophores compared to that of the MoO_2L_2 complex (Table 1). Elongation of $d_{N=N}$ (~0.04 Å) distance(s) and shortening of

Table 3. Crystallographic Data for the Complexes 1, 2, and $[\mathbf{2}]I_3$

	1	**2**	$[\mathbf{2}]I_3$
empirical formula	$C_{38}H_{48}MoN_6O_4$	$C_{38}H_{48}CrN_6O_2$	$C_{38}H_{48}CrN_6O_2I_3$
molecular mass	748.76	672.82	1053.52
temperature (K)	293	293	293
crystal system	monoclinic	monoclinic	monoclinic
space group	$P2_1/n$	$C2/c$	$P2_1/c$
a (Å)	10.8445(8)	18.210(3)	19.983(6)
b (Å)	13.501(1)	15.258(2)	10.545(3)
c (Å)	25.2225(18)	17.196(3)	20.782(6)
α (deg)	90	90	90
β (deg)	95.156(2)	113.908(4)	92.786(9)
γ (deg)	90	90	90
V (Å^3)	3677.9(5)	4367.9(12)	4374(2)
Z	4	4	4
D_{calcd} (g/cm^3)	1.352	1.023	1.600
cryst. dimens. (mm)	0.14 × 0.16 × 0.18	0.08 × 0.12 × 0.16	0.08 × 0.10 × 0.12
θ range for data coll. (deg)	1.6−31.3	1.8−23.8	2.0−22.8
GOF	1.02	1.06	0.90
reflns. collected	56 191	22 665	41 341
unique reflns.	11 608	3330	5803
final R indices [$I > 2\sigma(I)$]	$R1$ = 0.0368 $wR2$ = 0.0832	$R1$ = 0.0371 $wR2$ = 0.1113	$R1$ = 0.0505 $wR2$ = 0.1589

d_{M-Nazo} are consistent with accumulation of negative charge on the azo groups and is an indication that the ligand(s) is/are reduced in this complex.[5,18] Molecular view with partial atom numbering scheme of the one-electron-oxidized complex $[\mathbf{2}]I_3$ is displayed in Figure 5b. The coordination geometry of the oxidized complex is similar to that of the neutral analogue, **2**. The most striking difference between the neutral **2** and cationic $[\mathbf{2}]I_3$ complexes is the significant contraction of the average N=N distances in the latter. Here the d_{N-N} (~1.29 Å) is shorter, and $d_{N(azo)-Cr}$ (~2.00 Å) is longer than the neutral isomer.

Cyclic Voltammetry and Electron Paramagnetic Resonance. The redox behaviors of the three aforenoted complexes were studied by cyclic voltammetry, and the data are collected in Table 4. Cyclic voltammetric experiments were performed in dichloromethane using tetrabutylammonium perchlorate (TBAP) as the supporting electrolyte; the reported potentials are all referenced to the Ag/AgCl electrode. The complex **1** showed one irreversible and a quasi-reversible cathodic response at −0.78 and −0.98 V, respectively (Supporting Information, Figure S5), which may be assigned to ligand-centered reductions[18] of the coordinated azo chromophores. The complex **2** showed two reversible

DOI: 10.1021/acs.inorgchem.5b00218
Inorg. Chem. 2015, 54, 5257−5265

Table 4. Selected Electrochemical and UV−vis Spectral Data

compound	cyclic voltammetric data[a] $E_{1/2}$[b], V (ΔE_p, mV)	UV−vis[e] λ_{max}[f](ε,10^4 $M^{-1}cm^{-1}$)
1	−0.78[d], −0.98[c]	570(0.39), 365 (0.51)
2	−0.27(100), 0.19(100)	670(0.11), 620(0.12), 410(0.39), 370(0.40), 295(0.59)
[**2**]I_3		610(0.26), 525(0.28), 415(0.55), 340(0.58)

[a]Dichloromethane solution (supporting electrolyte $[Bu_4N]ClO_4$), working electrode platinum, reference electrode Ag/AgCl. [b]$E_{1/2}$ = 0.5(E_{pa} + E_{pc}) where E_{pa} and E_{pc} are anodic and cathodic peak potentials, respectively, $\Delta E_p = E_{pa} - E_{pc}$, scan rate 50 mV s^{-1}. [c]Quasi-revesible [d]Irreversible. [e]Wavelength in nanometer; [f]Molar extinction coefficient in M^{-1} cm^{-1}in dichloromethane solvent.

responses: one oxidative and one reductive response at 0.19 and −0.27 V, respectively (Figure 6). The one-electron redox processes were confirmed by constant-potential electrolysis for the reversible waves at 0.40 and −0.45 V, respectively.

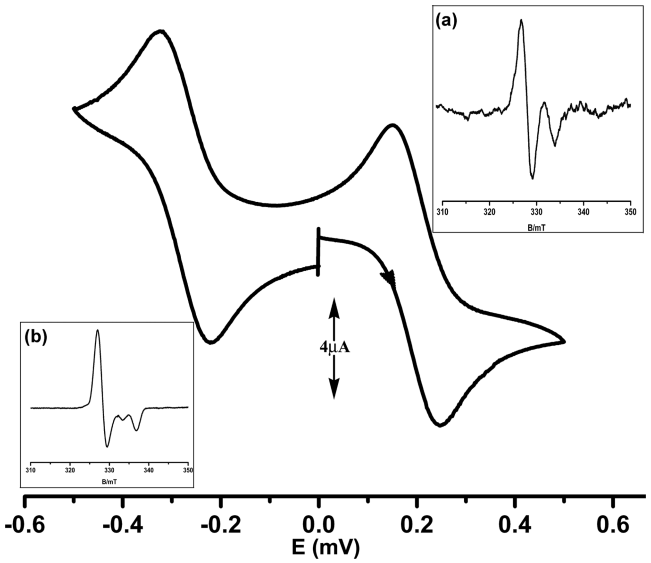

Figure 6. Cyclic voltammogram of **2**. (inset) EPR spectra of electrogenerated complexes: (a) [**2**]$^+$ and (b) [**2**]$^-$.

The oxidized complex [**2**]$^+$ (S = 3/2) and the reduced complex [**2**]$^-$ (S = 1/2) generated by exhaustive electrolysis of **2** were diagnosed by EPR spectroscopy at 120 K. The spectra showed (Figure 6, inset) metal-centered axial signals: at $g_\perp$ = 1.989, $g_\parallel$ = 1.955 (for [**2**]$^+$) and at $g_\perp$ = 1.986, $g_\parallel$ = 1.936 (for [**2**]$^-$) indicating that redox events are ligand centered in both cases and notably, their EPR spectra are similar. This is not surprising since the oxidized complex, [**2**]$^+$ (S = 3/2) undergoes zero-field splitting and splits into two Kramer's doublets (with m_s = ± 1/2 and m_s = ± 3/2). The ground Kramer's doublet (with m_s = ± 1/2) is responsible for the observed EPR line (due to a transition from m_s = −1/2 to m_s = +1/2) state. As the zero-field splitting is usually fairly large for Cr^{3+}, the higher Kramer's doublet (with m_s = ± 3/2) does not have any observable effect on the EPR spectrum.

Electronic Structure Analysis. To have a closer look into the electronic structures, we optimized the geometries of the complexes MoO_2L_2 and $[Cr(L)_2]^z$ (z = 0, ± 1) using B3LYP function, which is implemented in G09W. The optimized structural parameters and coordinates are given in Tables 1 and 2 and Supporting Information (Tables S1 and S2), respectively. The optimized metrical parameters matched well with that of experimentally observed values.

The broken-symmetry BS(3,1) solution and the spin-unrestricted (S = 1) solution for the neutral Cr-complex were found to be identical. Moreover UB3LYP for the neutral complex **2** (S = 1) converged to BS(3,1) solutions, and the optimized structure of the complex **2** agrees well with the experimentally observed one. The S = 1 ground state is attained by strong antiferromagnetic coupling of the single unpaired electron on the ligand with one of the three unpaired spins in the t_{2g} orbital of the Cr(III) center. The MO diagram (Figure 7) clearly indicates that three predominately metal d orbitals,

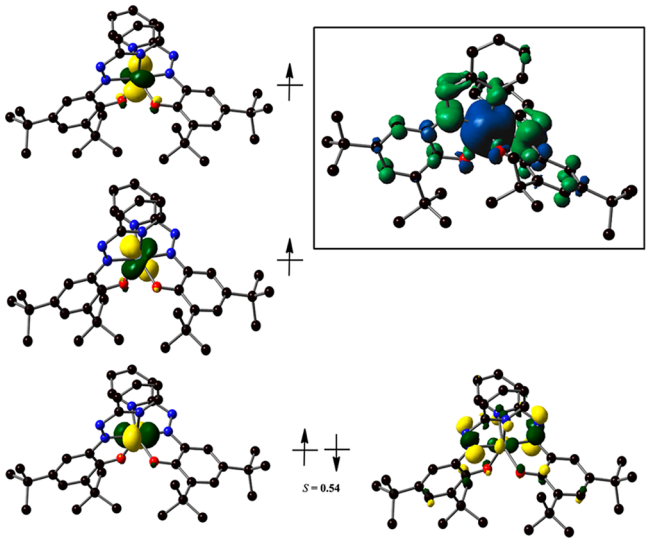

Figure 7. Qualitative MO diagram of the magnetic orbitals derived from BS(3,1) calculation of **2**. The spatial overlap (S) of the corresponding α and β orbitals is shown.

identified in CrL_2, are Cr-based orbitals and have originated from the t_{2g} set in an octahedral symmetry and occur in the spin-up manifold that defines a Cr(III) configuration (S_{Cr} = 3/2) of the metal center. The ligand spin is delocalized over the two ligands pointing to a formal charge of 1.5− for each ligand. A localized description[19] with two different oxidation states of the ligands, specifically, **2**$^-$ and **1**$^-$, is a more acceptable proposition though such oxidation states are impossible to identify because the two resonating forms are isoenergetic. The calculated Mulliken spin density plot (Figure 7, inset) showed that α-spin density of ∼2.84 electron spin at the Cr(III) center and a net β-spin density of ca. −0.84 on the two ligands. Accordingly, the electronic structure of **2** is best described as $[Cr^{III}(L^{1-})(L^{\bullet 2-})]$. However, there is another possible description of structure **2**: $[Cr^{II}(L^{1-})_2]$, which is eliminated by photoelectron spectroscopic study (see Supporting Information; Figure S6). The compound **2** showed a broad Cr 2p peak near 576.2 ± 0.1 eV, which compares well with the literature values for the known Cr(III) compounds.[20]

The optimized one-electron-oxidized complex [**2**]$^+$ generates a quartet ground state. The spin density at the metal is similar to that of the reduced complex, which indicates that the oxidation process is a ligand-based event and parallels the experimental findings. Thus, the structural impact is localized primarily in the ligand array where there are contraction of N═N distances (∼0.03 Å) (0.04 Å in the X-ray data) and

DOI: 10.1021/acs.inorgchem.5b00218
Inorg. Chem. 2015, 54, 5257−5265

elongation of Cr−N_{azo} bond lengths. The MO description of the oxidized complex showed that three metal-based orbitals are singly occupied and these are originated from the t_{2g} set of the central Cr atom. The spin-density plot and MO diagram are shown in Figure 8.

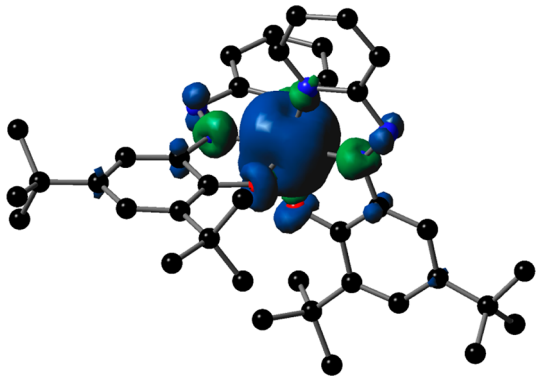

Figure 8. Spin-density plot of $[2]^{+}$.

One-electron-reduced complex $[Cr^{III}(L^{\bullet 2-})_2]^{-}$ is again a broken-symmetry BS(3,2) doublet. The MO diagram (Figure 9) showed three singly occupied metal d orbitals (>90%) and are originated from the t_{2g} set of the central Cr atom. The two metal spins antiferromagnetically coupled with two ligand radical spins resulting in overall one unpaired spin at the metal center and manifested a doublet ground state (vide EPR spectrum of $[2]^{-}$). The structural impact here again is localized in the ligand array where there is elongation of N═N distances (~0.02 Å on each ligand compared with neutral complex). The spin density plot and MO diagram are shown in Figure 9. All these taken together indicate that the Cr^{III} ion remains invariant across the entire series: $[CrL_2]^{0/+1/-1}$ with all redox phenomena occur at the ligand center. Similar ligand-centered redox events in homoleptic chromium complexes of 2,2′-bipyridine and 2-(arylazo)pyridine ligands were reported in the literature.[21,16c]

Time-dependent (TD) DFT calculations were performed to assign the origin of electronic transition of the complexes. The complex **1** is intensely blue colored and absorbed at 570 nm (Supporting Information, Figure S7). On the basis of the values of the oscillator strength, predicted by using TD-DFT, the most intense lowest energy transition at 570 nm is ascribed as intraligand charge transfer transition (ILCT): the oxygen atom and the phenyl group are the donors (highest occupied molecular orbital (HOMO−1)), while the π^* of azo (-N═N-) (lowest unoccupied molecular orbital (LUMO+1)) acts as acceptor (Figure S8 and Table S3).

The complex $[Cr^{III}(L^{1-})(L^{\bullet 2-})]$ showed a broad absorption at 670 nm, which is assigned as HOMO(α) → LUMO+1(α) (65%) transition at ca. 640 nm. HOMO(α) and LUMO+1(α) are primarily ligand orbitals (Figure S9). The oxidized compound $[Cr^{III}(L^{1-})_2]I_3$ is intensely green and absorbed at 610 nm, which is due to HOMO−1(α) → LUMO(α) (56%) transition where both orbitals are again ligand-based. The orbitals associated with these transitions are shown in Supporting Information, Figure S10, and values are tabulated in Supporting Information, Table S3.

Comments on the Formation of $[Mo^{VI}O_2(L^{1-})_2]$. Formation of the Mo(VI)-dioxo complex (**1**) from a chemical reaction between $Mo(CO)_6$ and 2HL in air is unusual and a rare case of formal oxidative addition of O_2 that proceeds via an intermediate brown complex (Scheme 2). However, our

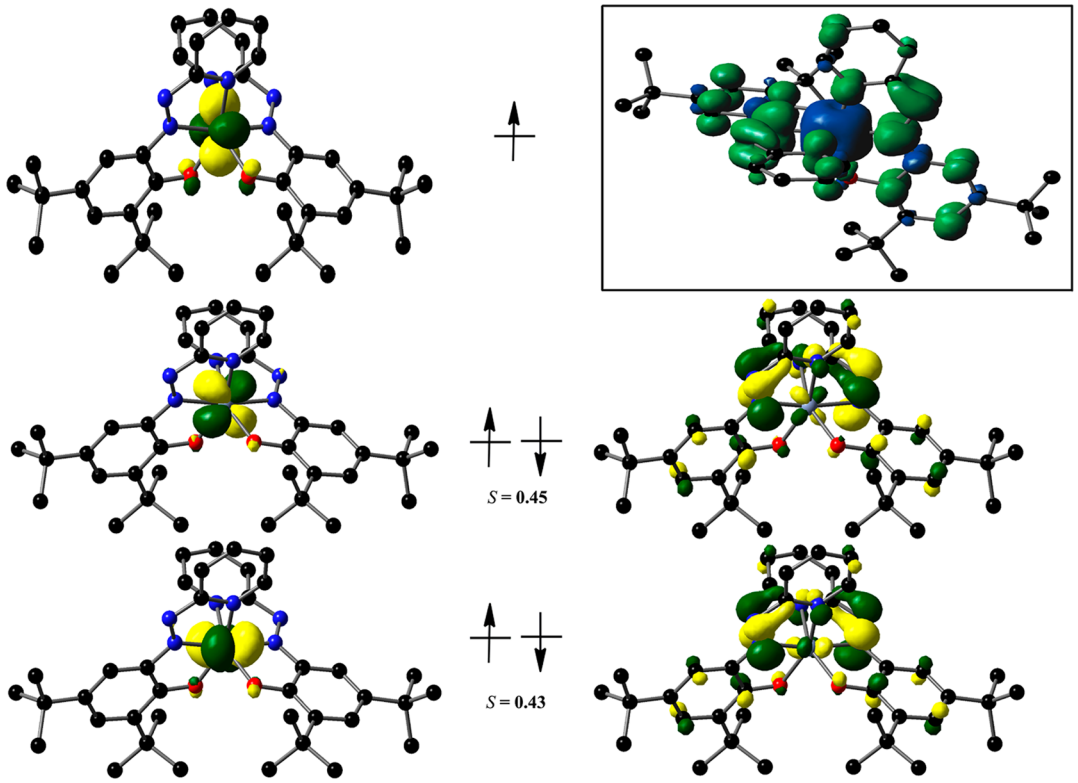

Figure 9. Qualitative MO diagram of the magnetic orbitals derived from BS(3,2) calculation of $[2]^{-}$. The spatial overlap (S) of the corresponding α and β orbitals is shown.

DOI: 10.1021/acs.inorgchem.5b00218
Inorg. Chem. 2015, 54, 5257−5265

present knowledge on the above reaction intermediate (brown complex) is not sufficient to assess the mechanism fully as yet.

Scheme 2

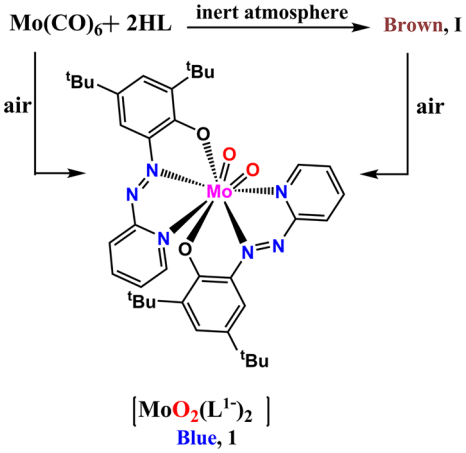

Nevertheless, a comparison of the results with the closely related systems, specifically, the present Cr-complex (**2**) and a similar Mo-complex (**3**) $[Mo^{IV}(L^{a\bullet 2-})_2]$ {HL^a = 2-[(2-*N*-arylamino)phenylazo]pyridine)} is worthwhile for the present purpose. The identity of the Cr-complex (**2**) has been discussed above, and the synthesis and characterization of the Mo-complex (**3**) from $Mo^0(CO)_6$ and HL^a was reported by us.[22]

Comparing the above results it appears that formation of the complex **1** goes via formal oxidative addition of O_2. However, note with caution that oxidative addition of O_2 involving a monometallic system is a spin-forbidden process.[23,24] In a similar situation, formation of a monometallic Cr-dioxo complex[23] was argued to go through a bimetallic intermediate, which was followed by mass-spectral analysis of distribution of the product of the chemical reaction in a mixture of equimolar quantity of $^{16}O_2$ and $^{18}O_2$. Our attempts for such a quantitative experiment were unsuccessful, and presently the mechanism of formation of **1** remains inconclusive.

CONCLUSION

In this report a rare case of octacoordinated *cis*-dioxo molybdenum(VI) is disclosed. Multiple electron-transfer processes are operative in producing the dioxo complex $[Mo^{VI}O_2(L^{1-})_2]$ from the chemical reaction of $Mo(CO)_6$ and 2HL in air. The geometry of this complex is a distorted square-antiprism. It is relevant to note that octacoordination in transition metal complexes[25] is rarely observed and that transition metal complexes with unusual coordination numbers have been of interest because of their occurrence in biology and also for understanding the participation of coordinatively saturated complexes in catalysis. A major highlight in the Cr complexes lies in the redox-noninnocent character of the ligand wherein the observed redox processes occur entirely at the ligand center without affecting the trivalent oxidation state of chromium. Thorough crystallographic, spectroscopic, and DFT analyses have been used to elucidate the electronic structures of the three redox isomers, namely, $[Cr^{III}(L^{1-})(L^{\bullet 2-})]$, $[Cr^{III}(L^{1-})_2]^+$, and $[Cr^{III}(L^{\bullet 2-})_2]^-$. Our further studies on OAT processes using the dioxo molybdenum complex are ongoing.

EXPERIMENTAL SECTION

Materials. The metal carbonyls $M(CO)_6$ (M = Cr, Mo) were Aldrich reagents, and *n*-octane was obtained from Spectrochem, India. The ligand HL was prepared by following a reported procedure.[26] Tetrabutylammonium perchlorate was prepared and recrystallized as reported earlier.[27] ***Caution!*** *Perchlorates must be handled with care and appropriate safety precautions!* All other chemicals and solvents were of reagent grade and were used as received.

Physical Measurements. Unless otherwise stated, syntheses of the complexes were made in open atmosphere. UV−vis absorption spectra were recorded on a PerkinElmer Lambda 950 UV−vis spectrophotometer. Infrared and NMR spectra were obtained using a Perkin−Elmer 783 spectrophotometer and a Bruker Avance 500 MHz spectrometer, respectively, and $SiMe_4$ was used as the internal standard. A PerkinElmer 240C elemental analyzer was used to collect microanalytical data (C, H, N). ESI mass spectra were recorded on a micromass Q-TOF mass spectrometer (serial no. YA263). Volatammetric measurements were performed under nitrogen atmosphere using a Ag/AgCl reference electrode, with a Pt disk working electrode and a Pt wire auxiliary electrode, in dichloromethane containing 0.1 M Bu_4NClO_4 in a PC-controlled PAR model 273A electrochemistry system. A Pt wire gauge working electrode was used for exhaustive electrolyses. $E_{1/2}$ for the ferrocenium−ferrocene couple under our experimental conditions was 0.40 V. X-ray photoelectron spectroscopy (XPS, Omicron, model 1712-62-11) measurements were done using an Al Kα radiation source under 15 kV voltage and 5 mA current conditions. The XPS spectra were referenced to the C−C/C−H component of the C_{1s} peak of the samples, assuming the binding energy of 285.0 eV. Temperature-dependent magnetic susceptibility measurements of **2** and [**2**]I_3 were performed with a Quantum-Design MPMS-XL-5 SQUID magnetometer equipped with a 5 T magnet in the range from 295 to 2 K at a magnetic field of 0.05 T. The experimental magnetic susceptibility data were corrected for underlying diamagnetism using Pascal's tabulated constants. EPR spectra in the X band were recorded with a JEOL JES-FA200 spectrometer.

Synthesis. *Synthesis of $[Mo^{VI}O_2(L^-)_2]$, **1**.* A mixture of 2,4-di-*tert*-butyl-6-(pyridin-2-ylazo)-phenol (HL) (235 mg, 0.76 mmol) and $[Mo(CO)_6]$ (100 mg, 0.38 mmol) in toluene (40 mL) was refluxed in air for 4 h. The solution gradually became ink-blue. Evaporation of this solution afforded a blue solid, which was subjected to purification by thin-layer chromatography on an alumina plate. With toluene as the eluent, a distinct blue band separated, which was extracted by methanol and collected by evaporation of the solvent. The blue compound, $[Mo^{VI}O_2(L^-)_2]$, **1**, was then crystallized by slow evaporation of its solution in dichloromethane−hexane (2:1) solvent mixture.

Yield: 78% (220 mg). Anal. Calcd for $C_{38}H_{48}MoN_6O_4$: C, 60.95; H, 6.46; N, 11.22. Found: C, 60.42; H, 6.39; N, 11.02%. ESI-MS: *m*/*z* 751.24 [**1**+H]$^+$. ^{1}H NMR (500 MHz; $CDCl_3$) δ ppm: 8.74 (d, 1H, *J* = 5.0); 8.06−8.03 (m, 2H); 7.55 (s, 1H); 7.33 (t, 1H, *J* = 6.0); 7.24 (s, 1H); 1.25 (s-CH_3, 9H); 0.78 (s-CH_3, 9H). IR, (KBr, cm^{-1}):1600 [ν(C═N) + ν(C═C)], 1375 [ν(N═N)] and 870 [ν(M=O).

In absolute deaerated conditions the above reaction produced a hyperactive brown solution (**I**), which on exposure to even trace of air converted fast to the blue complex **1**.

*Synthesis of $[Cr^{III}(L^{1-})(L^{\bullet 2-})]$, **2**.* A mixture of 2,4-di-*tert*-butyl-6-(pyridin-2-ylazo)-phenol (HL) (283 mg, 0.90 mmol) and $[Cr(CO)_6]$ (100 mg, 0.45 mmol) in *n*-octane (40 mL) was refluxed in air for 5 h. The solution gradually became green. Evaporation of this solution afforded a green solid, which was subjected to purification by thin-layer chromatography on an alumina plate. With toluene as the eluent, a distinct green band separated, which was extracted by methanol and collected by evaporation of the solvent. The green compound, $[Cr^{III}(L^{1-})(L^{\bullet 2-})]$, **2** was finally crystallized by slow evaporation of its solution of dichloromethane−methanol (1:1) solvent mixture.

Yield: 31% (94 mg). IR (KBr, cm^{-1}): 1602 [ν(C═N) + ν(C═C)], 1224 [ν(N═N)]. Anal. Calcd. for $C_{38}H_{48}CrN_6O_2$: C, 67.83; H, 7.19; N, 12.49. Found: C, 68.08; H, 7.26; N, 12.33%. ESI-MS: *m*/*z* 673 [**2**]$^+$.

DOI: 10.1021/acs.inorgchem.5b00218
Inorg. Chem. 2015, 54, 5257−5265

Synthesis of $[Cr^{III}(L^{1\cdot-})_2]I_3$, **[2]**$I_3$. To a 15 mL dichloromethane solution of the preformed complex **2** (50 mg, 0.074 mmol), a solution of iodine in the same solvent (40 mg in 5 mL) was added dropwise with constant stirring. The solution gradually became bright green. On solvent evaporation a dark mass was obtained, which was thoroughly washed with hexane to remove excess iodine. The crude product was purified through crystallization by the slow evaporation of its solution in dichloromethane−hexane (2:1) solvent mixture. Yield: 89%. IR (KBr, cm^{-1}): 1600 [ν(C═N) + ν(C═C)], 1360 [ν(N═N)]. ESI-MS: m/z 673 $[\mathbf{2}]^+$. Anal. Calcd for $C_{38}H_{48}CrN_6O_2I_3$: C, 43.32; H, 4.59; N, 7.98. Found: C, 43.12; H, 4.51; N, 7.85%.

X-ray Crystallography. Crystallographic data for the compounds **1**, **2**, $[\mathbf{2}]I_3$ are collected in Table 3. Suitable X-ray-quality crystals of these compounds are obtained by the slow evaporation of a dichloromethane−hexane solution of the respective compounds. All data were collected on a Bruker SMART APEX-II diffractometer, equipped with graphite-monochromated Mo Kα radiation (λ = 0.710 73 Å), and were corrected for Lorentz polarization effects. Unfortunately, the data sets for compound **2** and $[\mathbf{2}]I_3$ are incomplete in terms of the range of 2θ used in the refinements; the molecular structures, nevertheless, present no unusual features and have been determined unambiguously. Our attempts to grow better crystals were unsuccessful. The routine SQUEEZE was applied to intensity data of the complex **2** to take into account the highly disordered solvent molecules.[28] The number of electrons found in the solvent-accessible void is close to that expected for hexane molecule in the unit cell.

1. A total of 56 191 reflections were collected, of which 11 608 were unique (R_{int} = 0.042), satisfying the $I > 2\sigma(I)$ criterion, and were used in subsequent analysis.

2. A total of 22665, reflections were collected, of which 3330 were unique (R_{int} = 0.044), satisfying the $I > 2\sigma(I)$ criterion, and were used in subsequent analysis.

[2]I_3. A total of 41 341, reflections were collected, of which 5803 were unique (R_{int} = 0.098).

The structures were solved by employing the SHELXS-97 program package[29] and were refined by full-matrix least-squares based on F^2 (SHELXL-97).[30] All hydrogen atoms were added in calculated positions.

Computational Details. All DFT calculations presented in this paper were performed using the Gaussian 09W program package.[31] Full geometry optimizations were performed without symmetry constraints. The vibrational frequency calculations were performed to ensure that the optimized geometries represent the local minima and that there are only positive eigenvalues. The hybrid B3LYP exchange-correlation functional[32] was used. The TZVP basis set[33] of triple-ζ quality with one set of polarization functions was used on Cr atom. The SDD basis set[34] with effective core potential was employed for the Mo atom. The 6-31G(d) basis set was employed for the C, H, N, and O atoms. The spin restricted and unrestricted calculations were performed for diamagnetic Mo complex and paramagnetic Cr complexes, respectively. The broken-symmetry approach[35,36] was employed to establish triplet and doublet state of the compounds **2** and $[\mathbf{2}]^-$, respectively. The calculations of the ground-state triplet/doublet were performed using spin-unrestricted approaches (in G09W, combined with guess = mix). Stability analysis of the wave functions were performed using the "stable = opt" keyword. Mulliken spin densities were used for analysis of the spin populations on ligand and metal centers.[37] Vertical electronic excitations based on B3LYP optimized geometries were computed using the TD-DFT formalism[38] in dichloromethane using conductor-like polarizable continuum model.[39] GaussSum[40] was used to calculate the percentage contribution of ligand and metal to the frontier orbital and the fractional contributions of various molecular orbital in the optical spectral transition.

■ ASSOCIATED CONTENT

Supporting Information

Simulated and experimental ESI-MS spectra, IR and UV-vis spectra, plot of μ_{eff} versus T, two planes of complex **1**, CV of complex **1**, XPS of complex **2**, frontier MO of complex **1**, contour plots of selected MOs, X-ray crystallographic file in CIF format. The Supporting Information is available free of charge on the ACS Publications website at DOI: 10.1021/acs.inorgchem.5b00218.

■ AUTHOR INFORMATION

Corresponding Author

*E-mail: icsg@iacs.res.in.

Author Contributions

†I.C. and N.S.C. contributed equally to this work.

Notes

The authors declare no competing financial interest.

■ ACKNOWLEDGMENTS

Financial support received from the Department of Science and Technology (DST, Project No. SR/S2/JCB-09/2011) and Council of Scientific and Industrial Research (Project No. 01(274)/13/EMR-II), New Delhi, is gratefully acknowledged. S.G. thanks DST for a J. C. Bose fellowship. Crystallography was performed at the DST-funded National Single Crystal Diffractometer Facility at the Department of Inorganic Chemistry, IACS. We thank Prof. S. Bhattacharya of Jadavpur Univ. for helpful discussions. I.C. and P.G. thank Council of Scientific and Industrial Research for fellowship support.

■ REFERENCES

(1) (a) Bandyopadhyay, P.; Bandyopadhyay, D.; Chakravorty, A.; Cotton, F. A.; Falvello, L. R.; Han, S. *J. Am. Chem. Soc.* **1983**, *105*, 6327−6329. (b) Mahapatra, A. K.; Bandyopadhyay, D.; Bandyopadhyay, P.; Chakravorty, A. *J. Chem. Soc., Chem. Commun.* **1984**, 999−1000. (c) Sinha, C. R.; Bandyopadhyay, D.; Chakravorty, A. *J. Chem. Soc., Chem. Commun.* **1988**, 468−470. (d) Paul, N. D.; Kramer, T.; McGrady, J. E.; Goswami, S. *Chem. Commun.* **2010**, *46*, 7124−7126.

(2) (a) Santra, B. K.; Lahiri, G. K. *J. Chem. Soc., Dalton Trans.* **1998**, 1613−1618. (b) Santra, B. K.; Thakur, G.; Ghosh, P.; Pramanik, A.; Lahiri, G. K. *Inorg. Chem.* **1996**, *35*, 3050−3052.

(3) (a) Panda, M.; Das, S.; Mostafa, G.; Castiñeiras, A.; Goswami, S. *Dalton Trans.* **2005**, 1249−1255. (b) Das, C.; Saha, A.; Hung, C.-H.; Lee, G.-H.; Peng, S.-M.; Goswami, S. *Inorg. Chem.* **2003**, *42*, 198−204. (c) Das, C.; Ghosh, A. K.; Hung, C.-H.; Peng, S.-M.; Lee, G.-H.; Goswami, S. *Inorg. Chem.* **2002**, *41*, 7125−7135. (d) Saha, A.; Majumdar, P.; Goswami, S. *J. Chem. Soc., Dalton Trans.* **2000**, 1703−1708. (e) Ghosh, A. K.; Majumdar, P.; Falvello, L. R.; Mostafa, G.; Goswami, S. *Organometallics* **1999**, *18*, 5086−5090.

(4) (a) Sengupta, D.; Ghosh, P.; Chatterjee, T.; Datta, H.; Paul, N. D.; Goswami, S. *Inorg. Chem.* **2014**, *53*, 12002−12013. (b) Deibel, N.; Schweinfurth, D.; Hohloch, S.; Fiedlerband, J.; Sarkar, B. *Chem. Commun.* **2012**, *48*, 2388−2390.

(5) (a) Shivakumar, M.; Pramanik, K.; Ghosh, P.; Chakravorty, A. *Chem. Commun.* **1998**, 2103−2104. (b) Doslik, N.; Sixt, T.; Kaim, W. *Angew. Chem., Int. Ed.* **1998**, *37*, 2403−2404.

(6) (a) Chatterjee, I.; Ghosh, P.; Datta, H.; Goswami, S. *Indian J. Chem.* **2014**, *53A*, 27−33. (b) Chatterjee, S.; Sanyal, A.; Hung, C.-H.; Goswami, S. *Z. Anorg. Allg. Chem.* **2007**, *633*, 1775−1777. (c) Lahiri, G. K.; Goswami, S.; Falvello, L. R.; Chakravorty, A. *Inorg. Chem.* **1987**, *26*, 3365−3370.

(7) Paul, N. D.; Samanta, S.; Mondol, T. K.; Goswami, S. *Inorg. Chem.* **2011**, *50*, 7886−7893.

(8) Sheldon, R. A.; Arends, I.; Hanefeld, U. *Green Chemistry and Catalysis;* Wiley-VCH: Weinheim, Germany, 2007.

(9) (a) Examples of such catalytic OAT process involving O_2 are limited though OAT process in general are commonly available. (b) Sharma, S. K.; May, P. S.; Jones, M. B.; Lense, S.; Hardcastle, K. I.; MacBeth, C. E. *Chem. Commun.* **2011**, *47*, 1827−1829. (c) Oya, K.;

DOI: 10.1021/acs.inorgchem.5b00218
Inorg. Chem. 2015, 54, 5257−5265

Seino, H.; Akiizumi, M.; Mizobe, Y. *Organometallics* **2011**, *30*, 2939−2946.
(10) (a) Usharani, D.; Janardanan, D.; Li, C.; Shaik, S. *Acc. Chem. Res.* **2013**, *46*, 471−482. (b) Bongards, C.; Gärtner, W. *Acc. Chem. Res.* **2010**, *43*, 485−495.. (c) Goldberg, D. P. *Acc. Chem. Res.* **2007**, *40*, 626−634.
(11) Tshuva, E. Y.; Lippard, S. J. *Chem. Rev.* **2004**, *104*, 987−1012.
(12) (a) Borovik, A. S.; Zinn, P. J.; Zart, M. K. *In Activation of Small Molecules: Organometallic and Bioinorganic Perspectives;* Tolman, W. B., Ed.; Wiley-VCH: Weinheim, Germany, 2006, 187−234. (b) Nam, W. *Acc. Chem. Res.* **2007**, *40*, 465−465. (c) Lippert, C. A.; Arnstein, S. A.; Sherrill, C. D.; Soper, J. D. *J. Am. Chem. Soc.* **2010**, *132*, 3879−3892. (d) Schax, F.; Bill, E.; Herwig, C.; Limberg, C. *Angew. Chem., Int. Ed.* **2014**, *53*, 12741−12745.
(13) Lippard, S. J. *Prog. Inorg. Chem.* **2007**, *21*, 91−103.
(14) (a) Chandra, U.; Gilbert, O.; Kumara Swamy, B. E.; Bodke, Y. D.; Sherigara, B. S. *Int. J. Electrochem. Sci.* **2008**, *3*, 1044−1054. (b) Tuncel, M.; Kahyaoglu, H. *Transition Met. Chem.* **2008**, *33*, 605−613. (c) Anderson, R. G.; Nickless, G. *Analyst* **1968**, *93*, 13−19.
(15) (a) Damme, N. V.; Lough, A. J.; Gorelsky, S. I.; Lemaire, M. T. *Inorg. Chem.* **2013**, *52*, 13021−13028. (b) Rajput, A.; Sharma, A. K.; Barman, S. K.; Koley, D.; Steinert, M.; Mukherjee, R. *Inorg. Chem.* **2014**, *53*, 36−48. (c) Damme, N. V.; Zaliskyy, V.; Lough, A. J.; Lemaire, M. T. *Polyhedron* **2015**, *89*, 155−159.
(16) (a) Goswami, S.; Sengupta, D.; Paul, N. D.; Mondal, T. K.; Goswami, S. *Chem.—Eur. J.* **2014**, *20*, 6103−6111. (b) Paul, N. D.; Rana, U.; Goswami, S.; Mondal, T. K.; Goswami, S. *J. Am. Chem. Soc.* **2012**, *134*, 6520−6523. (c) Joy, S.; Krämer, T.; Paul, N. D.; Banerjee, P.; McGrady, J. E.; Goswami, S. *Inorg. Chem.* **2011**, *50*, 9993−10004. (d) Paul, N.; Samanta, S.; Goswami, S. *Inorg. Chem.* **2010**, *49*, 2649−2655. (e) Sanyal, A.; Chatterjee, S.; Castiñeiras, A.; Sarkar, B.; Singh, P.; Fiedler, J.; Záliš, S.; Kaim, W.; Goswami, S. *Inorg. Chem.* **2007**, *46*, 8584−8593. (f) Sanyal, A.; Banerjee, P.; Lee, G−H.; Peng, S−M.; Hung, C−H.; Goswami, S. *Inorg. Chem.* **2004**, *43*, 7456−7462. (g) Samanta, S.; Singh, P.; Fiedler, J.; Záliš, S.; Kaim, W.; Goswami, S. *Inorg. Chem.* **2008**, *47*, 1625−1633.
(17) (a) Korstanje, T. J.; Folkertsma, E.; Lutz, M.; Jastrzebski, J. T. B. H.; Gebbink, R. J. M. K. *Eur. J. Inorg. Chem.* **2013**, 2195−2204. (b) Karunadasa, H. I.; Chang, C. J.; Long, J. R. *Nature* **2010**, *464*, 1329−1333.
(18) (a) Ghosh, B. K.; Chakravorty, A. *Coord. Chem. Rev.* **1989**, *95*, 239−294. (b) Samanta, S.; Ghosh, P.; Goswami, S. *Dalton Trans.* **2012**, *41*, 2213−2226.
(19) (a) Scarborough, C. C.; Lancaster, K. M.; DeBeer, S.; Weyhermüller, T.; Sproules, S.; Wieghardt, K. *Inorg. Chem.* **2012**, *51*, 3718−3732. (b) Lesh, F. D.; Lord, R. L.; Heeg, M. J.; Bernhard, H. S.; Verani, C. N. *Eur. J. Inorg. Chem.* **2012**, 463−466. (c) Ghosh, P.; Samanta, S.; Roy, S. K.; Demeshko, S.; Meyer, F.; Goswami, S. *Inorg. Chem.* **2014**, *53*, 4678−4686.
(20) Kemnitz, E.; Kohne, A.; Grohmann, I.; Lippitz, A.; Unger, W. E. S. *J. Catal.* **1996**, *159*, 270−279.
(21) Scarborough, C. C.; Sproules, S.; Weyhermüller, T.; DeBeer, S.; Wieghardt, K. *Inorg. Chem.* **2011**, *50*, 12446−12462.
(22) Sanyal, A.; Chatterjee, S.; Castiñeiras, A.; Sarkar, B.; Singh, P.; Fiedler, J.; Záliš, S.; Kaim, W.; Goswami, S. *Inorg. Chem.* **2007**, *46*, 8584−8593.
(23) Dai, F.; Yap, G. P. A.; Theopold, K. H. *J. Am. Chem. Soc.* **2013**, *135*, 16774−16776.
(24) Howe, P. R.; McGrady, J. E. *Inorg. Chem.* **2002**, *41*, 2026−2031 and references therein.
(25) Patra, A. K.; Dube, K. S.; Papaefthymiou, G. C.; Conradie, J.; Ghosh, A.; Harrop, T. C. *Inorg. Chem.* **2010**, *49*, 2032−2034.
(26) (a) Campbell, N.; Henderson, A. W.; Taylor, D. *J. Chem. Soc.* **1953**, 1281−1285. (b) Anderson, R. G.; Nickless, G. *Anal. Chim. Acta* **1967**, *39*, 469−477.
(27) Goswami, S.; Mukherjee, R. N.; Chakravorty, A. *Inorg. Chem.* **1983**, *22*, 2825−2832.
(28) van der, S. P.; Spek, A. L. *Acta Crystallogr., Sect. A: Found. Crystallogr.* **1990**, *46*, 194−201.
(29) Sheldrick, G. M. *Acta Crystallogr., Sect. A* **1990**, *46*, 467−473.
(30) Sheldrick, G. M. *SHELXL 97,* Program for the refinement of crystal structures; University of Göttingen: Göttingen, Germany, 1997.
(31) Frisch, M. J.; Trucks, G. W.; Schlegel, H. B.; Scuseria, G. E.; Robb, M. A.; Cheeseman, J. R.; Montgomery, J. A., Jr.; Vreven, T.; Kudin, K. N.; Burant, J. C.; Millam, J. M.; Iyengar, S. S.; Tomasi, J.; Barone, V.; Mennucci, B.; Cossi, M.; Scalmani, G.; Rega, N.; Petersson, G. A.; Nakatsuji, H.; Hada, M.; Ehara, M.; Toyota, K.; Fukuda, R.; Hasegawa, J.; Ishida, M.; Nakajima, T.; Honda, Y.; Kitao, O.; Nakai, H.; Klene, M.; Li, X.; Knox, J. E.; Hratchian, H. P.; Cross, J. B.; Bakken, V.; Adamo, C.; Jaramillo, J.; Gomperts, R.; Stratmann, R. E.; Yazyev, O.; Austin, A. J.; Cammi, R.; Pomelli, C.; Ochterski, J. W.; Ayala, P. Y.; Morokuma, K.; Voth, G. A.; Salvador, P.; Dannenberg, J. J.; Zakrzewski, V. G.; Dapprich, S.; Daniels, A. D.; Strain, M. C.; Farkas, O.; Malick, D. K.; Rabuck, A. D.; Raghavachari, K.; Foresman, J. B.; Ortiz, J. V.; Cui, Q.; Baboul, A. G.; Clifford, S.; Cioslowski, J.; Stefanov, B. B.; Liu, G.; Liashenko, A.; Piskorz, P.; Komaromi, I.; Martin, R. L.; Fox, D. J.; Keith, T.; Al-Laham, M. A.; Peng, C. Y.; Nanayakkara, A.; Challacombe, M.; Gill, P. M. W.; Johnson, B.; Chen, W.; Wong, M. W.; Gonzalez, C.; Pople, J. A. *Gaussian 09,* Revision C.01; Gaussian, Inc.: Wallingford, CT, 2010.
(32) (a) Becke, A. D. *J. Chem. Phys.* **1993**, *98*, 5648−5652. (b) Lee, C.; Yang, W.; Parr, R. G. *Phys. Rev. B: Condens. Matter Mater. Phys.* **1988**, *37*, 785−789. (c) Vosko, S. H.; Wilk, L.; Nusair, M. *Can. J. Phys.* **1980**, *58*, 1200−1211. (d) Stephens, P. J.; Devlin, F. J.; Chabalowski, C. F.; Frisch, M. J. *J. Phys. Chem.* **1994**, *98*, 11623−11627.
(33) Schäfer, A.; Huber, C.; Ahlrichs, R. *J. Chem. Phys.* **1994**, *100*, 5829−5835.
(34) (a) Andrae, D.; Haeussermann, U.; Dolg, M.; Stoll, H.; Preuss, H. *Theor. Chim. Acta* **1990**, *77*, 123−141. (b) Fuentealba, P.; Preuss, H.; Stoll, H.; Szentpaly, L. V. *Chem. Phys. Lett.* **1982**, *89*, 418−422.
(35) Ginsberg, A. P. *J. Am. Chem. Soc.* **1980**, *102*, 111−117.
(36) (a) Noodleman, L.; Case, D. A.; Aizman, A. *J. Am. Chem. Soc.* **1988**, *110*, 1001−1005. (b) Noodleman, L.; Davidson, E. R. *Chem. Phys.* **1986**, *109*, 131−143. (c) Noodleman, L.; Norman, J. G., Jr.; Osborne, J. H.; Aizman, C.; Case, D. A. *J. Am. Chem. Soc.* **1985**, *107*, 3418−3426. (d) Noodleman, L. *J. Chem. Phys.* **1981**, *74*, 5737−5743.
(37) Mulliken, R. S. *J. Chem. Phys.* **1955**, *23*, 1833−1840.
(38) (a) Bauernschmitt, R.; Ahlrichs, R. *Chem. Phys. Lett.* **1996**, *256*, 454−464. (b) Stratmann, R. E.; Scuseria, G. E.; Frisch, M. J. *J. Chem. Phys.* **1998**, *109*, 8218−8224. (c) Casida, M. E.; Jamoroski, C.; Casida, K. C.; Salahub, D. R. *J. Chem. Phys.* **1998**, *108*, 4439−4449.
(39) (a) Cossi, M.; Rega, N.; Scalmani, G.; Barone, V. *J. Comput. Chem.* **2003**, *24*, 669−681. (b) Cossi, M.; Barone, V. *J. Chem. Phys.* **2001**, *115*, 4708−4717. (c) Barone, V.; Cossi, M. *J. Phys. Chem. A* **1998**, *102*, 1995−2001. (d) O'Boyle, N. M.; Tenderholt, A. L.; Langner, K. M. *J. Comput. Chem.* **2008**, *29*, 839−845.
(40) Leininger, T.; Nicklass, A.; Stoll, H.; Dolg, M.; Schwerdtfeger, P. J. *J. Chem. Phys.* **1996**, *105*, 1052−1059.

DOI: 10.1021/acs.inorgchem.5b00218
Inorg. Chem. 2015, 54, 5257−5265